

# Joint well-placement and well-control optimization for energy-efficient water flooding of oil fields

I Gusti Agung Gede Angga<sup>a</sup>, Per Eirik Strand Bergmo<sup>b</sup>, Carl Fredrik Berg<sup>a,\*</sup>

<sup>a</sup> Department of Geoscience and Petroleum, Norwegian University of Science and Technology (NTNU), S. P. Andersens veg 15A, 7031, Trondheim, Norway

<sup>b</sup> Department of Petroleum, SINTEF Industry, S. P. Andersens veg 15B, 7031, Trondheim, Norway

## ARTICLE INFO

### Keywords:

Energy efficiency  
Carbon emission reduction  
Water flooding  
Well placement optimization  
Well control optimization  
Collaborative optimization algorithm

## ABSTRACT

Hydrocarbon production driven by water flooding is energy-intensive. This paper presents well-placement and joint well-placement-and-control optimization studies with objective function taking into account CO<sub>2</sub> emissions, pursuing more energy-efficient water flooding. To assess the effect of emission cost on the optimal drainage strategy, multiple optimization problems implementing different CO<sub>2</sub> tax levels are solved. The solutions for higher tax levels usually inject less water and proportionally emit less CO<sub>2</sub>. The trade-off between emissions and oil production is non-linear: For lower tax levels, we obtain solutions providing large emission reductions with limited reductions in production. Increasing the CO<sub>2</sub> tax further, any additional emission reduction leads to a larger reduction in oil production due to reduced opportunities for energy efficiency. Enforcement of higher tax levels usually produces optimal drainage strategies with higher injection effectiveness and lower emission intensity. However, some increases in CO<sub>2</sub> tax, particularly above the critical level, have negligible impact on the optimal solution, hence they only affect the profitability negatively without further reducing emissions or improving emission intensity. Compared to the well-placement solutions, the solutions for our joint optimization emit less CO<sub>2</sub> and provide higher profit. They also have lower emission intensity due to lower injection pressure. The adjustable well-control enables our joint optimization to stop field production after some years which could be more profitable than continuing the production at high CO<sub>2</sub> tax. These clearly demonstrate the advantages of incorporating the well-control variables, giving more freedom to our joint optimization. In well-placement optimization, reductions in water injection and emissions are obtained by decreasing well productivity and injectivity and by increasing inter-well distance. In joint optimization, water injection can also be reduced by adjusting the well-control, hence there is no clear trend in well productivity and inter-well distance with changes in injection volume. The trends in well characteristics concluded from the well-placement solutions could mislead the search for more energy-efficient drainage as they are different from the trends observed in the joint optimization solutions, indicating the importance of joint optimization in this study.

## 1. Introduction

Production of oil and gas is energy-intensive, and thus the production leads to large emissions. According to Rystad Energy in 2019, the upstream oil and gas activities accounted for ~2% of the global CO<sub>2</sub> emissions (Rystad Energy, 2019). They also indicate that, in large oil-producing countries like Norway, the upstream petroleum sector even took the largest portion of domestic greenhouse gas emissions, e.g., ~28% in 2017 (Rystad Energy, 2019). Around 85% of the CO<sub>2</sub> emissions from the Norwegian petroleum sector come from the fuel combustion in gas turbines that power up both offshore and onshore facilities (Rystad Energy, 2019). For typical offshore oil fields on the Norwegian Continental Shelf, water injection is the most energy-intensive

operation where it constitutes around 50% power demand (Svalheim and King, 2003). A lot of energy is used for lifting water from the subsurface reservoir to the topside facility, separating and treating the produced water, as well as re-injecting the water for pressure support.

The world was facing an energy crisis in 2022 and fossil fuels will still be needed in the upcoming years. On the other hand, the world is also facing a climate crisis and many have urged for more aggressive climate change mitigation actions to reduce emissions. To deal with both crises, there is a need for maintaining the production of oil and gas to meet the increasing energy demand while at the same time lowering the CO<sub>2</sub> emissions from the production process. One potential solution for this tough challenge is energy efficiency, particularly in the area of

\* Corresponding author.

E-mail addresses: [i.g.a.g.angga@ntnu.no](mailto:i.g.a.g.angga@ntnu.no) (I.G.A.G. Angga), [per.bergmo@sintef.no](mailto:per.bergmo@sintef.no) (P.E.S. Bergmo), [carl.f.berg@ntnu.no](mailto:carl.f.berg@ntnu.no) (C.F. Berg).

<https://doi.org/10.1016/j.geoen.2023.212251>

Received 10 March 2023; Received in revised form 11 July 2023; Accepted 13 August 2023

Available online 16 August 2023

2949-8910/© 2023 The Author(s). Published by Elsevier B.V. This is an open access article under the CC BY license (<http://creativecommons.org/licenses/by/4.0/>).

water management. Aligning with the recommendations given by the OG21 (OG21, 2022), improving the efficiency of water management should be prioritized as it offers a large room for reducing energy use and thus CO<sub>2</sub> emissions. An approach for improving water management efficiency is by optimizing the reservoir drainage so that it has less water injection and production, and hence lower emissions, as these three quantities are correlated.

Our earlier study focuses on obtaining energy-efficient drainage strategies by optimizing the well-control, i.e., well rates or bottom hole pressures throughout the field production period (Angga et al., 2022b). We propose a scheme for estimating CO<sub>2</sub> emissions of a particular injection strategy and employ it when defining the optimization objective. We also investigate how different emission costs affect the optimal injection strategies and their energy use. Enforcing higher emission costs on the objective would produce more energy-efficient injection strategies as indicated by lower injection volume, CO<sub>2</sub> emissions, and emission intensity. Another study of ours is about the optimization of inflow control valves under different lifting and injection costs (Angga et al., 2022c). By imposing higher lifting and injection costs on the net present value calculation (the optimization objective), we would obtain optimal configurations of the inflow control valves that reduce water production and injection as well as delay water breakthrough. From both studies, we notice that the more energy-efficient drainage strategies will have reduced production, but it is relatively small compared to the reductions in water production and injection, which correlate with a reduction in CO<sub>2</sub> emissions. This work, on the other hand, concentrates on optimizing different types of variables that define subsurface drainage, i.e., the well-placement and joint well-placement-and-control.

Location and trajectory of production and injection wells are critical decisions in the development of oil and gas fields because they will impact the reservoir drainage and thus the asset profitability. Optimization of well-placement is often deemed as a challenging problem; it is more challenging than well-control optimization as reservoir heterogeneity leads to non-smooth and non-convex objective functions having many local optima (see examples of objective function surfaces in Onwunalu and Durlafsky (2010) and Al Dossary and Nasrabadi (2016)). Well-placement optimization has been studied for years, and many optimization algorithms have been developed and tested for solving well-placement optimization problems efficiently. Islam et al. review the development of well-placement optimization problems, as well as the application of various optimization methods for solving them (Islam et al., 2020). In addition to well location, the control schedule of production and injection wells throughout the field lifetime is an equally important decision in field development because it is influencing the subsurface drainage too, and thus affecting the CO<sub>2</sub> emissions as shown in Angga et al. (2022b). Optimizing well-placement and well-control individually or sequentially will likely produce sub-optimal drainage strategies (Bellout et al., 2012; Li and Jafarpour, 2012), and this has motivated researchers to investigate joint optimization of well-placement-and-control, herein referred to as “joint optimization”. To date, there are several works that develop and test out different approaches for solving joint optimization problems, e.g., in Li et al. (2013), Isebor et al. (2014), Forouzanfar et al. (2016), Lu and Reynolds (2020), Sayyafzadeh and Alrashdi (2020) and Semnani et al. (2021). In terms of optimization objectives, most well-placement and joint optimization studies in the literature are single-objective optimization problems. There are different kinds of objective functions, for instance, profit or net present value (NPV) as in Kristoffersen et al. (2022) and Chen et al. (2022), oil production or recovery factor as in Hutahean et al. (2014), productivity index as in Ding (2008), Theil index as in Chen et al. (2018), and displacement vector parameter as in Chen et al. (2017). Some of these objectives might be conflicting, which makes multi-objective optimization an active area of research to identify trade-offs between different objectives. For example in Rostamian et al. (2019) and Siddiqui et al. (2015), the authors solve for multi-objective optimization problems considering NPV and recovery factor

as objectives, and then demonstrate the non-dominated solutions, also called the Pareto set, for both objectives.

To our knowledge, only a few well-placement or joint optimization studies consider environmental aspects in their optimization objectives. One of them is the work of Awotunde and Sibaweih (2014), where the authors use voidage replacement ratio (VRR), i.e., the ratio of injection volume to production volume, as an objective beside NPV in a multi-objective optimization problem. According to the paper, VRR could be used as an indicator for assessing the environmental impact of field production, and the ratio is preferably maintained close to unity in order to prevent environmental problems caused by pressure imbalance. Nevertheless, aiming VRR close to unity is not a proper objective when searching for energy-efficient subsurface drainage. For example, when water channeling occurs in a reservoir due to its heterogeneity, we will likely have  $VRR \approx 1$ , but that circumstance will consume a lot of energy because a significant amount of water needs to be lifted to the topside facility and re-injected into the reservoir. Naderi and Khamehchi perform joint well-placement-and-control optimization to minimize water production and then determine the sensitivity of the optimization variables (Naderi and Khamehchi, 2017). They point out that water production will decrease with increased tubing head pressure and shortened perforation length. The optimization study is carried out using water-drive gas reservoirs, meaning that the production is supported by natural energy in the reservoirs and the energy use on the topside facility might be insignificant. In contrast, the work herein considers oil reservoirs supported with energy-intensive water injection, as this is an important target for emission reductions. In our earlier study (Angga et al., 2022d), we examined the effect of well-placement on the CO<sub>2</sub> emissions from water flooding operations, further we investigated the effect of emission cost on the optimal well-placement. That study concentrated on the placement of a vertical injector in 2D reservoir models, while this present study employs a 3D model and optimizes both producer and injector placement with freedom on the well orientation. According to our earlier study, the injector placement in a more permeable area would result in more energy-efficient drainage because the injection pressure needed to achieve the given rate target is lower.

The aforementioned knowledge gap has motivated us to conduct this study. Contributions of the present study to the existing knowledge body are summarized as follows:

- We formulate and solve a well-placement optimization problem, where we optimize the placement of both production and injection wells in a water flooding operation. Most importantly the optimization here includes the cost of CO<sub>2</sub> emissions as part of the objective function, allowing us to obtain drainage strategies with low carbon emissions.
- To assess the effect of emission cost on the optimal well-placement, we solve multiple optimization problems implementing different CO<sub>2</sub> tax levels using the novel collaborative algorithm introduced in Angga et al. (2022a). The trade-offs between emissions and production or NPV in different optimal solutions are then studied.
- We investigate the characteristics of the wells that can potentially lower the energy used. The examined characteristics consist of perforation length, permeability surrounding the wells, well productivity or injectivity, and inter-well distance.
- The results of the well-placement optimization have encouraged us to extend this study by also incorporating the well-control as decision variables, meaning that we also deal with a joint well-placement-and-control optimization problem.

This paper is structured as follows: Section 2 explains the methodology of the present study; including methods for well construction, reservoir simulation, CO<sub>2</sub> emissions estimation, NPV calculation, and optimization. Section 3 provides the details of both well-placement and joint optimization problems to solve, as well as the description of the

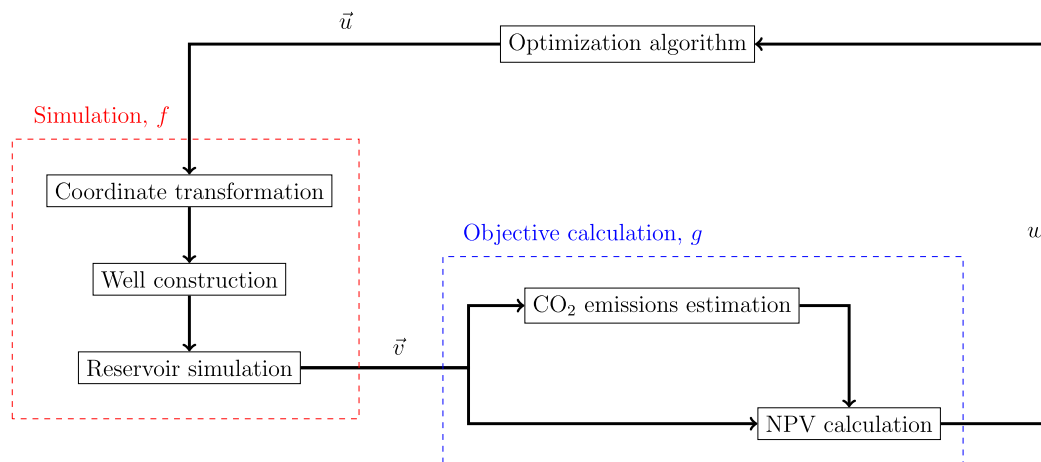


Fig. 1. A flowchart of the optimization loop. The vector  $\bar{u}$  is a set of decision variables to evaluate. The vector  $\bar{v} = f(\bar{u})$  is outputs of a model simulation,  $f$ , with respect to  $\bar{u}$ . Lastly, the variable  $w = g(\bar{v})$  is a value of objective function,  $g$ , with respect to  $\bar{v}$ .

reservoir model employed. Section 4 presents the optimization results and discusses them. Lastly, Section 5 gives the concluding remarks of this study.

## 2. Methodology

A flowchart of the optimization process is depicted in Fig. 1. The process commences with an optimization algorithm deciding a set of variable values,  $\bar{u}$ , to be evaluated. In well-placement optimization,  $\bar{u}$  consists of heel and toe coordinates that define the production and injection wells, whereas in joint optimization,  $\bar{u}$  also contains rate and bottom hole pressure targets that control the wells. The evaluation of  $\bar{u}$  is divided into two parts: First, a model simulation,  $f$ , with respect to  $\bar{u}$  is carried out. Second, the simulation results,  $\bar{v} = f(\bar{u})$ , are exploited for an objective calculation,  $g$ ; giving us an objective value,  $w = g(\bar{v})$ , which will be fed back to the optimization algorithm and used for deciding the next test candidate  $\bar{u}$ . This optimization loop repeats until one stopping criterion is met. As indicated by the red box in Fig. 1, the simulation,  $f$ , comprises three sub-routines, i.e., coordinate transformation, well construction, and reservoir simulation. These sub-routines will be discussed further in Section 2.1. For the objective calculation,  $g$ , CO<sub>2</sub> emissions that correspond to  $\bar{v}$  are first estimated and then used for an NPV calculation (see the blue box in Fig. 1). These two calculations are described in Section 2.2. The simulation process,  $f$ , particularly the reservoir simulation part, is computationally more demanding than the objective calculation,  $g$ . We therefore employ an optimization algorithm that can take advantage of such characteristics. Details of the optimization algorithm are given in Section 2.3

### 2.1. Simulation

In this work, coordinates of the well heel and toe are expressed in the natural coordinate system, and we adopt the iso-parametric mapping (Bathe, 1982) for transforming a natural coordinate  $(\xi, \eta, \zeta)$  to a global Cartesian coordinate  $(x, y, z)$ . The iso-parametric mapping, which is widely used in finite element analysis, is a one-to-one mapping (Murthi and Valliappan, 1986). By definition, the variables  $\xi, \eta, \zeta$  in the natural coordinate system can vary from  $-1$  to  $1$ , and these lower and upper bounds define our search space in optimization. The reason for expressing well coordinates in the natural coordinate system is to facilitate defining a physical search space in the global Cartesian coordinate system; herein we only need eight nodes for defining a physical search space. The formulation of iso-parametric mapping for an 8-node hexahedral element is available in Yuan et al. (1994), Zhou et al. (2017) and Li et al. (2014).

The well herein is defined by the global Cartesian coordinates of the well heel and toe, and the well path is a straight line stretching from the well heel to its toe. To our knowledge, the reservoir simulator that we employed cannot directly use the well path defined in the Cartesian coordinates for simulation. The simulator requires well completion data consisting of (i) the grid blocks that are in connection with the wells and their (I, J, K) indexes, (ii) the order of the connections, and (iii) the transmissibility factor for each connection between the wellbore and the reservoir grid block. Actually, the connection factor can be computed by the simulator based on the grid block size, permeability, and the wellbore radius, however, since the well might penetrate only a fraction of the grid block or might not be situated in the center of the grid block, the connection factor should be provided in order to get the right inflow properties. Typically, the well path defined in the Cartesian coordinates is translated into the well completion data using industry-standard reservoir modeling software. Instead of using commercial software, we utilize the *WellIndexCalculator* feature of the open-source optimization framework *FieldOpt* (Petroleum Cybernetics Group NTNU, 2021) for generating the well completion data from the Cartesian coordinates of the well heel and toe. This well construction sub-routine is repeated for all production and injection wells considered for optimization. Next, a reservoir simulation is carried out using the well completion data that have been generated. For this sub-routine, we employ the open-source reservoir simulator *Flow* by OPM (2022a).

### 2.2. Objective calculation

Once the model simulation is complete, the simulation results,  $\bar{v}$ , are input for an objective calculation. For that, CO<sub>2</sub> emissions of a drainage strategy under specific well-placement and well-control are first estimated using a CO<sub>2</sub> emission calculator presented in Angga et al. (2022b). The emission calculator integrates subsurface reservoir, surface injection network, and topside facility models. The calculator utilizes the simulation results,  $\bar{v}$ , in particular the injector bottom hole pressure and injection rate profiles, as inputs. These profiles are needed for estimating the head and flow rate required from the pumping system. The required head and flow rate are then used for determining the optimal pumping system configuration, including the optimal pump rate and the optimal number of pumps running in parallel and in series so that the power consumption of the pumping system is minimized. The power consumption of the water treatment system is estimated based on the injection rate profile as well. Power consumption of both pumping and water treatment systems makes up the total power demand. Note that the energy used for lifting up the produced fluid from the subsurface reservoir is not yet taken into account in the emission calculator. Using the total power demand, the calculator then

decides the configuration of the power generation system, including the number of gas turbines needed and their part-load power output and efficiency. Lastly, the amounts of fuel combusted in the gas turbines and the CO<sub>2</sub> emissions associated with the combustion process are estimated. Details and assumptions of the CO<sub>2</sub> emission calculator are given in Angga et al. (2022b).

The simulation results,  $\bar{v}$ , and the estimated fuel consumption and CO<sub>2</sub> emissions are used for evaluating the objective function of our well-placement and joint optimization problems. Herein the optimization problems aim to maximize the net present value (NPV) defined as follows:

$$NPV(\bar{v}) = -I_0(\bar{v}) + \sum_{t=1}^T \left[ \frac{CF_t(\bar{v})}{(1+d)^t} \right] - V_p(\bar{v}) \quad (1a)$$

$$I_0(\bar{v}) = C_d \times L_w(\bar{v}) \quad (1b)$$

$$CF_t(\bar{v}) = R_t(\bar{v}) - O_t(\bar{v}) - T_t(\bar{v}) \quad (1c)$$

$$R_t(\bar{v}) = P_o \times N_{p,t}(\bar{v}) \quad (1d)$$

$$O_t(\bar{v}) = C_w \times W_{i,t}(\bar{v}) + C_f \times G_{f,t}(\bar{v}) \quad (1e)$$

$$T_t(\bar{v}) = r_{CO_2} \times G_{CO_2,t}(\bar{v}) \quad (1f)$$

where the variable  $I_0$  represents the initial investment for drilling the wells, and it is a product of the unit drilling cost,  $C_d$ , and the total length of all the wells,  $L_w$ . The length of a well is approximated by adding up (i) the Euclidean distance between the well heel and toe global coordinates with (ii) the true vertical depth of the well heel location. The cash flow in year- $t$ ,  $CF_t$ , is equal to the revenue,  $R_t$ , minus the operating expenses,  $O_t$ , and the CO<sub>2</sub> tax,  $T_t$ . The revenue in year- $t$ ,  $R_t$ , is calculated by multiplying the oil price,  $P_o$ , with the total volume of oil produced in year- $t$ ,  $N_{p,t}$ . The operating expenses in year- $t$ ,  $O_t$ , consist of two components, i.e., the cost of treating the injected water and the cost of fuel combusted in the gas turbines. The former component is a product of the unit water treatment cost,  $C_w$ , and the total volume of water injected in year- $t$ ,  $W_{i,t}$ . The latter component is obtained by multiplying the unit cost of fuel,  $C_f$ , with the total amount of fuel used in year- $t$ ,  $G_{f,t}$ . The latter component herein reflects the cost of the injection itself because the fuel consumption,  $G_{f,t}$ , will vary depending on the power demand for running the injection pumps and water treatment systems. In order to replace the volume of oil produced, the amount of water injected is usually larger than the water produced, and we therefore assume that all the produced water will be re-injected. We do not include a term responsible for treating the produced water in Eq. (1e) because all costs related to water treatment have already been accounted for in  $C_w \times W_{i,t}$ . The CO<sub>2</sub> tax in year- $t$ ,  $T_t$ , depends on the CO<sub>2</sub> tax level,  $r_{CO_2}$ , and the cumulative CO<sub>2</sub> emissions in year- $t$ ,  $G_{CO_2,t}$ . The future cash flows,  $CF_t$ , are discounted to the present time using a discount rate,  $d$ . The discounted cash flows throughout the field lifetime,  $T$ , are summed up to form the NPV. The variable  $V_p$  in Eq. (1a) denotes the penalty value. It is equal to an arbitrarily large number when the injection strategy is not achievable by the pumping system, and it is equal to zero otherwise.

### 2.3. Optimization algorithm

One of the goals of the present study is to evaluate the effect of emission cost on optimal well-placement. In order to fulfill the goal, we define and solve multiple optimization problems that embed different CO<sub>2</sub> tax levels,  $r_{CO_2}$ , for the NPV calculation. Since the optimization problems implement different CO<sub>2</sub> tax levels, each optimization problem,  $P_i$ , has a unique objective function,  $h_i$ . The collection of  $N_p$  different optimization problems forms a so-called multi-task optimization (MTO) problem. In the MTO context, an optimization problem,  $P_i$ , is usually referred to as a “task”. The purpose of MTO is not to find the trade-offs among different objectives,  $h_i$ , but to fully and simultaneously optimize each task so that the relationship between different tasks

can be exploited for improving the search process of each task (Gupta et al., 2016). The outcome of an MTO problem is a set of optimal solutions,  $\{\bar{u}_1^*, \bar{u}_2^*, \dots, \bar{u}_{N_p}^*\}$ , where  $\bar{u}_i^*$  denotes an optimal solution for the optimization problem  $P_i$ , or it is mathematically expressed as  $\bar{u}_i^* = \text{argmax}_{\bar{u}_i \in \Omega} h_i(\bar{u}_i)$  for a maximization problem. An overview of MTO and a list of relevant solvers can be found in Osaba et al. (2022).

In our MTO problems, the evaluation of the objective function,  $h_i$ , is carried out in two stages: First, a simulation of the reservoir model,  $f$ , with respect to the decision variables  $\bar{u}$  is performed. Second, the simulation outputs,  $\bar{v} = f(\bar{u})$ , are exploited for computing the objective function,  $g$ . In our case, the objective calculation,  $g$ , comprises estimating the CO<sub>2</sub> emissions and then calculating the NPV. Because each optimization problem,  $P_i$ , enforces a specific CO<sub>2</sub> tax level,  $r_{CO_2,i}$ , the objective calculation,  $g_i$ , is therefore unique. The full expression of the objective evaluation process is given as  $h_i(\bar{u}) = g_i \circ f(\bar{u})$ , where  $f$  is independent of the tax level  $r_{CO_2,i}$ . The model simulation,  $f$ , is a computationally heavy operation, while the objective calculation,  $g_i$ , has a light computation cost.

Having the 2-stage objective evaluation process with the heavy/light-function structural characteristic, where only the light function  $g_i$  is problem specific, we herein employ the collaborative optimization framework (Angga et al., 2022a). The framework can take advantage of the objective evaluation process characteristic, and thus can solve our MTO problems more efficiently. In particular, the collaborative optimization framework has two distinctive features: First, the framework solves all optimization problems defined in our MTO simultaneously. Second, the framework performs a collaborative operation every single iteration, where in this particular operation the results of heavy model simulation,  $\bar{v}$ , are shared among all search processes, thus enhancing the information available for deciding the next candidate solutions in any search process. With these distinctive features, the collaborative optimization framework is likely to converge faster than traditional search methods, meaning that the collaborative algorithm needs fewer iterations and thus fewer computationally-heavy reservoir simulations to find the optimal solutions,  $\{\bar{u}_1^*, \bar{u}_2^*, \dots, \bar{u}_{N_p}^*\}$ . For this study, we use the collaborative version of the genetic algorithm (C-GA) with  $N_p$  populations acting in concert; each population is assigned to tackle one optimization problem in our MTO. The collaborative operation in the C-GA intends to replace the worst members of a population with better individuals cloned from other populations so that the genetic information of the population is getting better. As demonstrated in Angga et al. (2022a,c), the C-GA often outperforms the standard non-collaborative genetic algorithm. We refer to the paper of Angga et al. (2022a) for further description of the collaborative optimization framework as well as the C-GA.

## 3. Description of optimization problems

### 3.1. Reservoir model

Before discussing the details of our well-placement and joint optimization problems in Sections 3.2 and 3.3, respectively, we will first describe the “Egg” model we use for this study. The Egg model, which was developed by Jansen et al. (2014), is a synthetic three-dimensional reservoir model with a heterogeneous permeability field representing channelized sand bodies. In Jansen et al. (2014), the Egg model is presented as an ensemble of 100 reservoir realizations having different permeability fields. Since this study focuses on working with a deterministic reservoir model, we employ only one of the realizations, in particular the first realization where the rock horizontal permeability varies as in Fig. 2. The Egg model is commonly used to simulate two-phase oil-water flow with water flooding as the main production mechanism due to the absence of an aquifer and gas cap. Note that all production and injection wells defined in the standard Egg model and their control parameters are excluded from this work. Besides, the field production period is shortened to six years in order to cut the

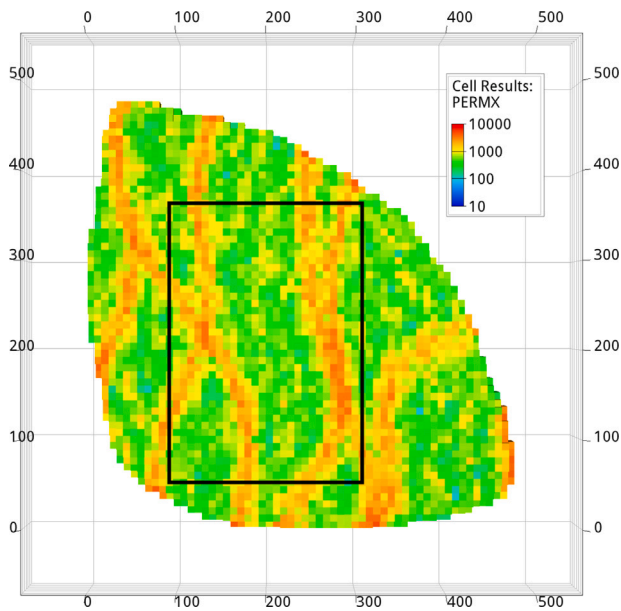


Fig. 2. Top view of the Egg model which has an egg-like shape and high-permeability channels in a low-permeability background. The grid block color represents the horizontal permeability (unit: mD). The rectangle outlined in black defines the search space in our well-placement and joint optimization problems. Visualization of the Egg model is carried out using the open-source reservoir simulation post-processing software *ResInsight* (OPM, 2022b).

simulation run time and reduce the number of well-control variables in the joint optimization. Other reservoir rock and fluid properties as well as simulation parameters are left unchanged as per the standard Egg model given in Jansen et al. (2014).

The horizontal permeability of the employed reservoir realization ranges from 10 to 10000 mD, whereas the vertical permeability is one-tenth of the horizontal permeability. The Egg reservoir model has homogeneous porosity of 20% and homogeneous initial water saturation of 10%. The reservoir lies between 4000 and 4028 meter subsurface with an initial reservoir pressure at the reservoir top of 400 bar. The presence of high-permeability channels in the Egg model (see Fig. 2) introduces tough challenges for water flooding operation, like an early water breakthrough. Such a situation could lead to recirculation of a significant amount of injected water, thus consuming much energy and emitting a large amount of CO<sub>2</sub> relative to the amount of produced resources. The placement of both production and injection wells is therefore a critical decision for the development of a channelized reservoir like the Egg model, and this becomes the primary reason for using the Egg model for this study. Besides its operational challenges, the Egg model is considered a small reservoir model with 60 × 60 × 7 grid blocks, of which 18553 grid blocks are active. The small model size makes the simulation time relatively short, i.e., on average about 60 s per simulation, and this makes our total optimization time reasonable. The other reason for using the Egg model herein is that the model has been widely used as a test case in many published optimization studies, for example in Arouri et al. (2022), Chen et al. (2022), Ng and Jahanbani Ghahfarokhi (2022) and Wang et al. (2022), and it is therefore preferable for comparisons.

### 3.2. Optimization problem #1: Well-placement optimization

In our well-placement optimization, there are one production well and one injection well of which their placement will be optimized. Each well is defined based on its heel and toe coordinates in three-dimensional space. Therefore, our well-placement optimization involves a total of 12 decision variables, i.e., 2 wells × 2 points for

each well (1 heel + 1 toe) × 3 coordinates for each point, which all compose the vector  $\vec{u}$ . As mentioned in Section 2.1, the coordinates of the well heel and toe are expressed in the natural coordinate system, and thus every variable in  $\vec{u}$  is constrained between  $-1$  and  $1$ . The transformation from the natural coordinate system to the global Cartesian coordinate system is completed using the iso-parametric mapping. The global Cartesian coordinates of the eight nodes needed for the coordinate transformation are listed in Table A.1. These coordinates define our physical search space as illustrated in Fig. 2 (the black-outlined rectangle). Modification of the physical search space can be achieved by simply adjusting the coordinates of the eight nodes. The production well is controlled to reach a constant bottom hole pressure (BHP) target of 300 bar throughout the production period of six years. In contrast, the injection well is primarily controlled with the rate mode, targeting a constant water injection rate of 5000 sm<sup>3</sup>/d. The injection control will be switched to the BHP mode if the injector BHP rises and reaches the assumed formation fracture pressure of 420 bar. Additionally, the radii of both production and injection wells are 0.1 m.

Regarding the estimation of CO<sub>2</sub> emissions, we use most parameters given in the paper of Angga et al. (2022b) for the emission calculator, except for the pumps and the gas turbines where both are resized to fit the small reservoir size. The pump performance curves, i.e., the rate-vs-head and the rate-vs-efficiency curves, as well as the gas turbine full-load power output, are herein scaled down by a factor of one-tenth. All parameters needed for the NPV calculation expressed in Eq. (1) are listed in Table A.2. To investigate the effect of emission cost on the optimal well-placement, 18 well-placement optimization problems implementing discrete CO<sub>2</sub> tax levels for their NPV calculations are defined and solved, forming an MTO problem with  $N_p = 18$ . The variants of CO<sub>2</sub> tax level,  $r_{CO_2}$ , ranging from 0 to  $1.3125 \times 10^4$  USD/ton are provided in Table A.2. In this study, the upper limit of the CO<sub>2</sub> tax level is set rather high in order to see how dramatic tax levels provoke clear changes in the optimal well-placement or well-control. Lastly, all parameters for the collaborative genetic algorithm (C-GA) employed in this study are found in Table A.3.

### 3.3. Optimization problem #2: Joint well-placement-and-control optimization

According to Farajzadeh et al. (2022, 2019), high water cut fields tend to have high emission intensity, indicating that they will emit more CO<sub>2</sub> per barrel of oil equivalent produced. The amount of CO<sub>2</sub> emissions also grows rapidly as the field water cut increases. So, besides our joint optimization problems which will be described next, we also solve well-placement optimization problems like the ones presented in Section 3.2, but with the implementation of a reactive measure for controlling the production well during the reservoir simulations. The reactive well-control measure will shut in the production well, and eventually the field, if the field water cut exceeds 95%, aiming to lessen the CO<sub>2</sub> emissions by means of limiting the water production and the need for re-injection. In these optimization problems, the number and the type of decision variables remain the same as the well-placement optimization problems described in Section 3.2.

For our joint optimization problems, instead of embedding the reactive well-control measure, we include the well-control setting as decision variables in addition to the well-placement variables, and then let the optimizer find the best configuration of well-placement-and-control. The well-control setting consists of the BHP targets for the production well and the rate targets for the water injection well. These targets can be changed every year over the six-year simulated production period, giving us 12 additional decision variables in the vector  $\vec{u}$ , i.e., 2 wells × 6 control periods. So, our joint optimization problems involve 24 decision variables in total, consisting of 12 well-placement variables and 12 well-control variables. The search for optimal BHP targets for the production well is confined to a range of 300 to 420 bar, while the search space for the injector rate targets is defined between

0 and 5000  $\text{sm}^3/\text{d}$ . The search space for the well-control variables has already covered the possibilities for shutting in the production well (when the BHP target is set to the highest possible reservoir pressure of 420 bar) and for stopping the injection (when the injection rate target is set to zero). Therefore, the reactive well-control measure is theoretically unnecessary for joint optimization problems as the effort for lowering the field water cut can be made by adjusting the well-control variables, and it will be done automatically by the optimizer. All parameters for the  $\text{CO}_2$  emissions estimation, the NPV calculation, and the optimization algorithm are identical to the parameters used in Section 3.2.

#### 4. Results and discussion

Before discussing the optimal solutions for our optimization problems and their field production, profitability, and  $\text{CO}_2$  emissions, we will briefly talk about the optimization process. Using the collaborative optimization algorithm, the search process is carried out until the optimization has reached its termination criteria. In this study, the optimization is performed using a single-core standard workstation. It takes around 8 days for solving the 18 well-placement optimization problems with different emission costs, whereas the joint optimization problems require about 31 days to solve due to the larger number of decision variables, so they need a larger population size and more iterations. Since the collaborative genetic algorithm employed is basically a stochastic search algorithm that involves randomness during the search process, the optimization is repeated three times with different initial population members. For each optimization problem implementing a particular  $\text{CO}_2$  tax level, we pick the best solution obtained from the three different runs. The optimization produces different optimal solutions for most optimization problems implementing different  $\text{CO}_2$  tax levels. It might indicate that the range and the distribution of the tax levels considered in this study (see Table A.2) are sufficient to diversify the response surfaces of the optimization problems.

In the collaborative optimization framework, several search processes run simultaneously, where one search process is devoted to one optimization problem in our multi-task optimization. The collaboration between the search processes is materialized through the sharing of results of the computationally-heavy reservoir simulations. We observe that, in the early iterations, a search process collaborates with any other search processes because the sampling for various problems is still spread across the search space. Conversely, in the later iterations where the different search processes start converging towards their individual optimal solutions, a search process mainly collaborates with other search processes that tackle optimization problems with similar  $\text{CO}_2$  tax levels. These behaviors also appear in Angga et al. (2022a), and further explanations can be found there.

##### 4.1. Optimization problem #1: Well-placement optimization

In this subsection, the solutions for the well-placement optimization problems described in Section 3.2 are presented and discussed. The optimal placements for the production and injection wells under the various  $\text{CO}_2$  tax levels are shown in Fig. 3. Looking at the figure, all the optimal well locations are inside the search space. The optimal well-placements are apparently close to the boundary of our search space, and if we look at Fig. 2, they are also close to the reservoir boundary. The effect of reservoir size on the optimal placement has also been investigated in this work, i.e., by making the grid block size ten times larger. We find out that, as long as the production period is long enough to have a water breakthrough during the simulation, the different reservoir sizes all have optimal well-placements near the boundary of the search space. The permeability contrast between the highly permeable channels and the low permeability background also seems to have no influence on the optimal well-placement given that a

water breakthrough occurs. Besides, we defined and solved five well-placement optimization scenarios, implementing different shapes of the search space, but herein we only present the findings from one scenario (with the search space illustrated in Fig. 2) because the findings from all scenarios are similar and not dependent on the shape of the search space.

The variation of the field water injection rate (FWIR) over the simulated production period is shown in Fig. 4(a). Each line in this figure corresponds to an optimal well-placement for a particular  $\text{CO}_2$  tax level that is indicated by the line color. We can see that in most optimal solutions (except for the lowest  $\text{CO}_2$  tax level), the injection well never meets the targeted injection rate of 5000  $\text{sm}^3/\text{d}$ , implying the injection well has been controlled with the BHP mode throughout the simulation because the injector BHP always hits its upper limit of 420 bar. The optimal well-placements for higher  $\text{CO}_2$  tax levels lead to lower injection rates. This observation suggests the opposite of what reservoir engineers usually aim for, i.e., operating the injection well at the maximum allowed injection rate in order to achieve better sweep efficiency and increase economic gain. The field water cut (FWCT) profile shown in Fig. 4(b) also indicates that the optimal well-placements for higher tax levels have later water breakthrough and lower water cut. Since the injection well is controlled with the constant BHP in most optimal solutions, the lower injection rates for higher  $\text{CO}_2$  tax levels imply that the wells might have lower productivity or injectivity. We will examine this hypothesis later in this paper.

Fig. 4(c) displays the profile of total power consumption for operating the injection pumps and the water treatment system,  $P_{tot}$ , whereas Fig. 4(d) shows the mass rate variation of the  $\text{CO}_2$  emissions,  $\dot{m}_{\text{CO}_2}$ . According to Angga et al. (2022b), power consumption for water flooding operations and the associated  $\text{CO}_2$  emissions are dependent on the injection rate and pressure. However, since the injection pressure is almost identical for the different optimal well-placements in this study, the power consumption and the  $\text{CO}_2$  emissions are mainly influenced by the injection rate, and we can see the two plots for both aspects resemble the injection rate profile. In the solution for the zero  $\text{CO}_2$  tax regime,  $r_{\text{CO}_2} = 0$  USD/ton, the total power consumption and the  $\text{CO}_2$  emissions drop a little near the end of the production period (see the darkest blue line in Figs. 4(c) and 4(d)) due to the decrease in injection pressure. Also in the solution for the zero  $\text{CO}_2$  tax regime, the total power consumption and the  $\text{CO}_2$  emissions jump at the end of the first year. This is because the increase in injection rate requires another injection pump to run in parallel, and this lowers the efficiency of both pumps. Under the zero  $\text{CO}_2$  tax level, the optimizer barely considers the pump performance degradation as it has a minor influence on the NPV, i.e., it only affects the fuel cost which is small compared to the production revenue. Different ranges of y-axis in Figs. 4(c) and 4(d) indicate that the gas turbine runs at lower part-load efficiency when delivering lower power output. Even though the solutions for higher  $\text{CO}_2$  tax levels lead to lower part-load efficiency, they still have lower  $\text{CO}_2$  emissions, thanks to the lower power consumption.

Fig. 5(a) illustrates how the total oil production for the entire field (FOPT) non-linearly correlates with the total water injection for the field (FWIT). Each point in this figure represents the total oil produced and water injected of an optimal well-placement for a particular  $\text{CO}_2$  tax level. Referring to the figure, the optimal well-placements for higher  $\text{CO}_2$  tax levels entail less water to be injected and consequently produce less oil. The total field water production (FWPT) has a linear relationship with the total water injection. According to Fig. 5(b), the total field  $\text{CO}_2$  emissions,  $G_{\text{CO}_2}$ , is also a linear function of the total water injection, FWIT, expressed as follows:

$$G_{\text{CO}_2} = 0.0016 \frac{\text{ton}}{\text{sm}^3} \times \text{FWIT} + 13624 \text{ ton} \quad (2)$$

The linear correlation between the two quantities is likely due to the similarity in injection pressure among the different optimal solutions. Due to the characteristics of the topside equipment efficiency curves, e.g., the gas turbine part-load efficiency which drops at lower power

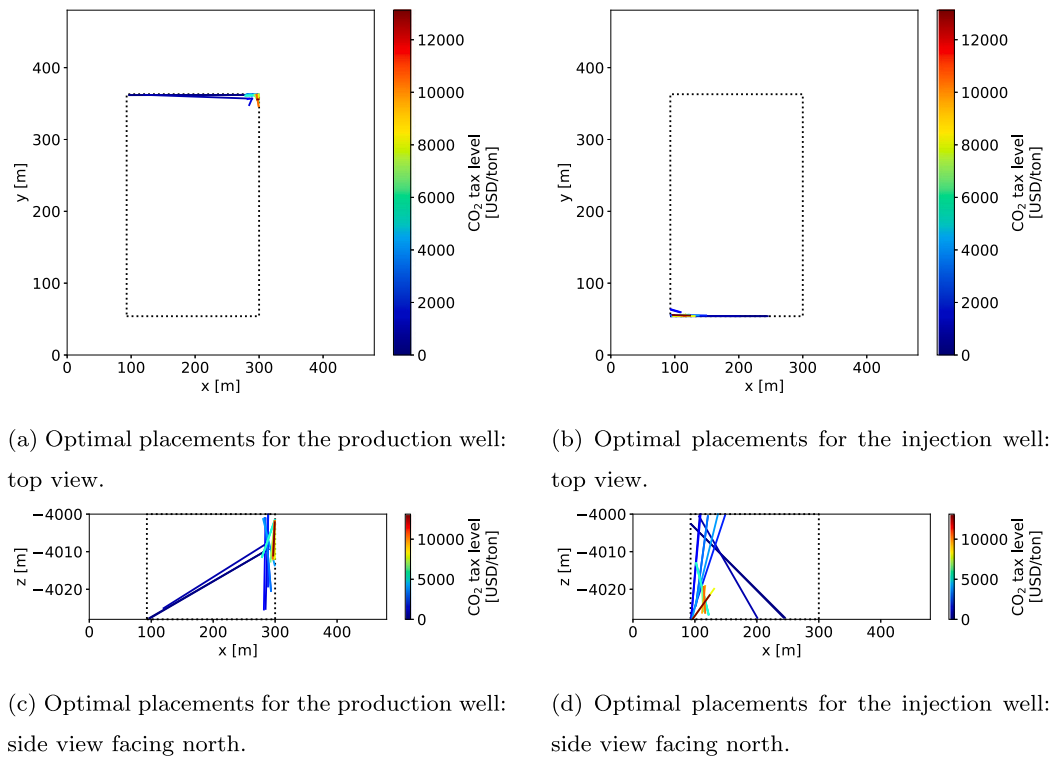


Fig. 3. Optimal placements for the production and injection wells for our well-placement optimization problems (see Section 3.2). The line color indicates the CO<sub>2</sub> tax level,  $r_{CO_2}$ , that an optimal well-placement is associated with. The rectangle with dotted outlines denotes the search space in our optimization problems.

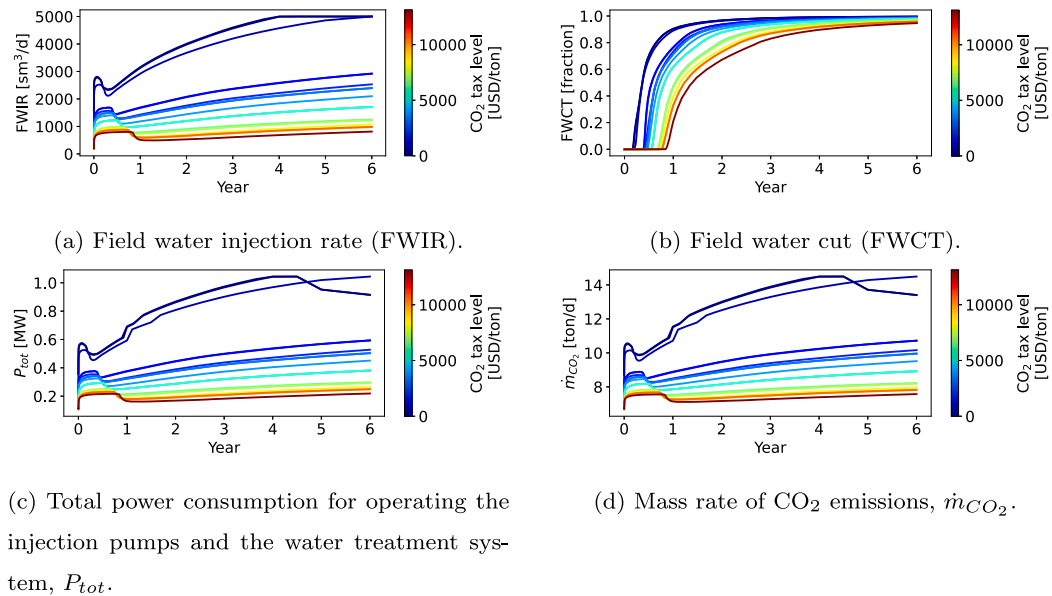


Fig. 4. Profile of field water injection rate, water cut, power consumption, and CO<sub>2</sub> emissions throughout the simulated production period with respect to different optimal solutions for our well-placement optimization problems implementing different CO<sub>2</sub> tax levels.

output, an extrapolation of the correlation above for zero injection volume will give a positive constant. The extrapolation is however not accurate because the emission model will actually result in zero CO<sub>2</sub> emissions when there is no water injection. Combining the relationships in Figs. 5(a) and 5(b), we have the relationship between the total CO<sub>2</sub> emissions and the total oil production shown in Fig. 5(c). It is evident that the two aspects are conflicting, meaning that the effort to reduce emissions will lessen oil production. The relationship is characterized by a steep slope on the right side of the plot, and the slope levels off towards the left side. The steeper slope on the right side implies

that, to a certain extent, we can have a large emission reduction with a small reduction in oil production. The return on energy efficiency measure diminishes as we move towards the left side of the plot. It means the same reduction in oil production will now give less reduction in emissions since the opportunities for energy efficiency become more limited. The relationship between CO<sub>2</sub> emissions and oil production is similar to what was observed in our previous works (Angga et al., 2022b,c).

The ratio between the amount of oil produced and the amount of water injected is referred to as “injection effectiveness”. As shown in

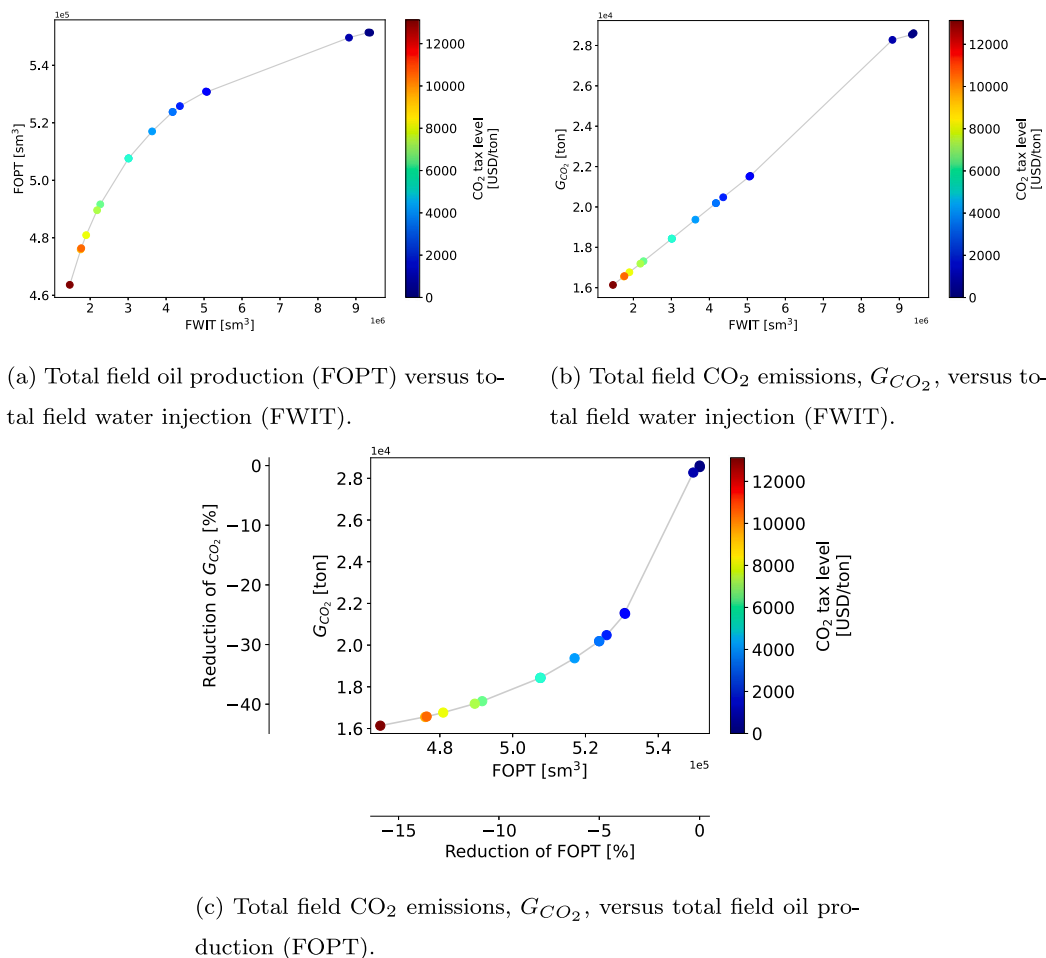


Fig. 5. Relationships between total field oil production, water injection, and CO<sub>2</sub> emissions that are constructed based on the optimal solutions for our well-placement optimization problems. The term “total” means cumulative throughout the simulated production period.

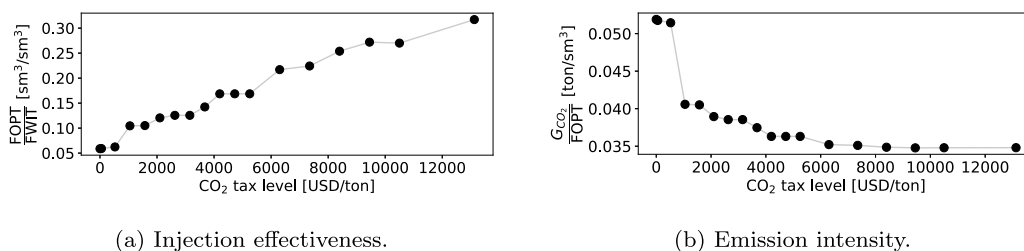


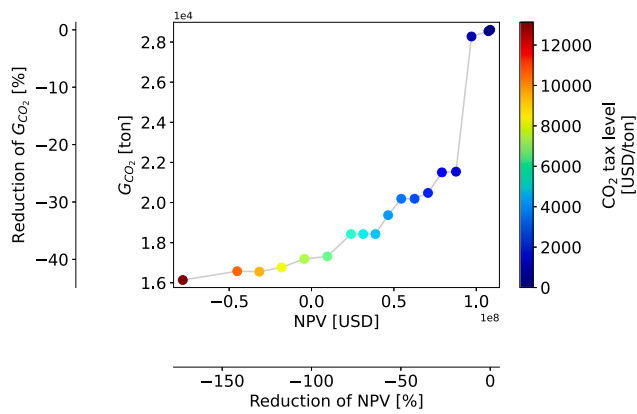
Fig. 6. Injection effectiveness and emission intensity of different optimal solutions for our well-placement optimization problems implementing different CO<sub>2</sub> tax levels.

Fig. 6(a), the injection effectiveness of different optimal solutions for increasing CO<sub>2</sub> tax level increases from 0.06 to 0.32. There is thus a clear trend that the optimal drainage strategies under higher CO<sub>2</sub> tax levels have better injection effectiveness. The amount of CO<sub>2</sub> emitted per unit volume of oil produced is called “emission intensity”. Fig. 6(b) indicates the emission intensity of different optimal well locations. With increasing CO<sub>2</sub> tax level, the emission intensity is reduced from 0.052 to 0.035 ton/sm<sup>3</sup>, equivalent to 8.3 and 5.5 kg CO<sub>2</sub> per barrel, respectively. The optimal well-placements for higher CO<sub>2</sub> tax levels usually offer lower emission intensity, but, in contrast to the injection effectiveness, the improvements in emission intensity taper off dramatically.

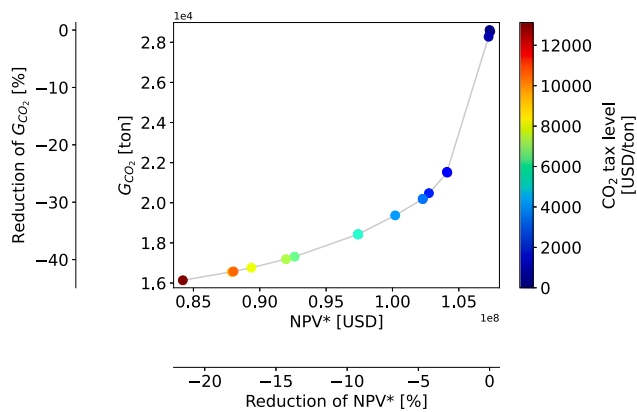
Fig. 7(a) is a plot showing the relation between the CO<sub>2</sub> emissions and the net present value (NPV). This plot might be interesting for government bodies who intend to make policies that can promote a large emission reduction while at the same time keeping the investment

return on hydrocarbon exploitation competitive. For example on the right part of the plot, an increase of CO<sub>2</sub> tax level to 1050 USD/ton, despite it causing the NPV to drop by ~19%, will result in an optimal well-placement with a significant emission reduction (~25%). Referring to some flat parts in Fig. 7(a), some increases in CO<sub>2</sub> tax level, e.g., from 4200 to 5250 USD/ton, are not effective because the tax increases only diminish the NPV without altering the optimal solutions and reducing the emissions. Lastly, increasing CO<sub>2</sub> tax level to 7350 USD/ton and above will turn the NPV negative, effectively stopping the field development.

Finding different optimal solutions for various emission costs is also a valuable investigation for operators, who need to plan for an uncertain CO<sub>2</sub> tax. For comparison, we let NPV\* be the NPV using the CO<sub>2</sub> tax level implemented in Norway in 2020 of 52.5 USD/ton (Tax Foundation, 2020). With NPV\*, operators can fairly compare different optimal well-placements obtained for various CO<sub>2</sub> tax levels. In



(a) Total field CO<sub>2</sub> emissions,  $G_{CO_2}$ , versus net present value (NPV).



(b) Total field CO<sub>2</sub> emissions,  $G_{CO_2}$ , versus NPV\*.

**Fig. 7.** Relationships between total field CO<sub>2</sub> emissions, NPV, and NPV\* that are constructed based on the optimal solutions for our well-placement optimization problems. For each optimal solution, the NPV in Fig. 7(a) is calculated using the CO<sub>2</sub> tax level associated with the solution. In contrast, the NPV\* in Fig. 7(b) is calculated using the CO<sub>2</sub> tax level implemented in Norway in 2020, i.e., 52.5 USD/ton (Tax Foundation, 2020).

Fig. 7(b), we plot the CO<sub>2</sub> emissions and the NPV\* of different optimal well locations. The trade-off between emissions and NPV\* is similar to the relationship between emissions and oil production (see Fig. 5(c)). Operators are interested in solutions that emit significantly less CO<sub>2</sub> without affecting the NPV\* too much. For example, the solution for  $r_{CO_2} = 2625$  USD/ton can lower the CO<sub>2</sub> emissions by ~29% while having a less than 5% drop on the NPV\*. The solutions for higher CO<sub>2</sub> tax levels might be less attractive to operators because the decreases in NPV\* become larger than the reductions in emissions.

Factors affecting the well productivity or injectivity are among others the perforation length,  $L_p$ , and the average permeability of the perforated section,  $\bar{K}_p$  (Adesina et al., 2011; Yuan et al., 2021). Fig. 8(a) indicates the relationship between the field water injection and the well productivity, in particular the product of  $\bar{K}_p$  and  $L_p$ . Referring to the figure, the production well tends to have lower productivity in the optimal solutions for higher CO<sub>2</sub> tax levels. The lower productivity would decrease the production rate, including the water production rate. Consequently, the injection volume needed for replacing the produced water will be smaller, and the CO<sub>2</sub> emissions will be less. Fig. 8(b) indicates how the field water injection correlates with the well injectivity in different optimal solutions. Similarly, the injection well tends to have lower injectivity in the optimal solutions for higher CO<sub>2</sub> tax levels. As discussed earlier, the injection control is switched to the

BHP mode because in any solution the injection pressure mostly rises up to its upper limit. Under the constant BHP injection mode, the lower injectivity will reduce the injection rate and hence the CO<sub>2</sub> emissions (see Figs. 4(a) and 4(d)). We also notice that the injectivity of the injection well is usually lower than the productivity of the production well.

The relationship between the water injection volume and the shortest inter-well distance is depicted in Fig. 8(c). The distance between the production and the injection wells is obtained using the algorithm for computing the shortest distance between two line segments available in Sunday (2021). Referring to the figure, the inter-well distance is usually larger in the optimal solutions for higher CO<sub>2</sub> tax levels. Together with the lower injection and production rates, the increase in inter-well distance will delay the water breakthrough (see Fig. 4(b)), and this will contribute to lessening the amount of produced water being re-injected and thus reducing the CO<sub>2</sub> emissions.

#### 4.2. Optimization problem #2: Joint well-placement-and-control optimization

Fig. 9 compares the emissions-versus-NPV relationships obtained from three different kinds of optimization: the well-placement optimization, the well-placement optimization with the reactive well-control measure, and the joint well-placement-and-control optimization. Compared to the solutions for the well-placement optimization, the inclusion of the reactive well-control can promote solutions that emit less CO<sub>2</sub> while having similar NPV, especially the solutions for lower CO<sub>2</sub> tax levels (e.g.  $r_{CO_2} \leq 1575$  USD/ton) which have large emission reductions ( $\geq 10\%$ ). For higher CO<sub>2</sub> tax levels, the solutions for well-placement optimization with and without the reactive well-control become more similar in terms of the NPV and the CO<sub>2</sub> emissions. The reason is that, for higher CO<sub>2</sub> tax levels, the well-placement optimization has lowered the well productivity and injectivity (see Figs. 8(a) and 8(b)) and increased the inter-well distance (see Fig. 8(c)), causing the production well to have a delayed water breakthrough and lower water cut (see Fig. 4(b)). In that circumstance, the reactive well-control measure becomes less effective in limiting water production and thus provides insignificant reductions in water injection and emissions.

As shown in Fig. 9, the solutions for our joint optimization usually have lower CO<sub>2</sub> emissions than the solutions for our well-placement optimization, either with and without the reactive well-control measure. For higher CO<sub>2</sub> tax levels (e.g.  $r_{CO_2} \geq 2100$  USD/ton), the solutions not only emit less CO<sub>2</sub> but even increase the NPV. This demonstrates the advantage of incorporating the well-control as decision variables in our joint optimization, as the solutions could improve the two conflicting objectives. For lower CO<sub>2</sub> tax levels (e.g.  $r_{CO_2} \leq 1575$  USD/ton), the reactive method is better than the joint optimization in terms of limiting the CO<sub>2</sub> emissions. This is a consequence of the rather coarse well-control in the joint optimization, i.e., only allowing for a change in well-control once a year. The reactive method does not have such a limitation, which makes it more efficient for lower CO<sub>2</sub> tax levels. The following will focus on discussing the solutions for our joint optimization and comparing them with the solutions for our well-placement optimization.

The optimal well-placements and well-controls for our joint optimization problems are illustrated in Figs. B.1 and B.2, respectively. We can see that all the optimal solutions are within the specified search space. Regarding the optimal well locations, they are all close to the boundaries of our search space and the reservoir, similar to the observation in Fig. 3. Additionally, the optimal solutions for  $r_{CO_2} \geq 2100$  USD/ton are almost identical, meaning that further increases in CO<sub>2</sub> tax level above 2100 USD/ton will not improve the drainage energy efficiency and therefore will not be effective in reducing the emissions, but they will still decrease the NPV.

Given the optimal well-controls shown in Fig. B.2, the actual variation of the field water injection rate (FWIR) over the simulated production period is depicted in Fig. 10(a). For higher CO<sub>2</sub> tax levels

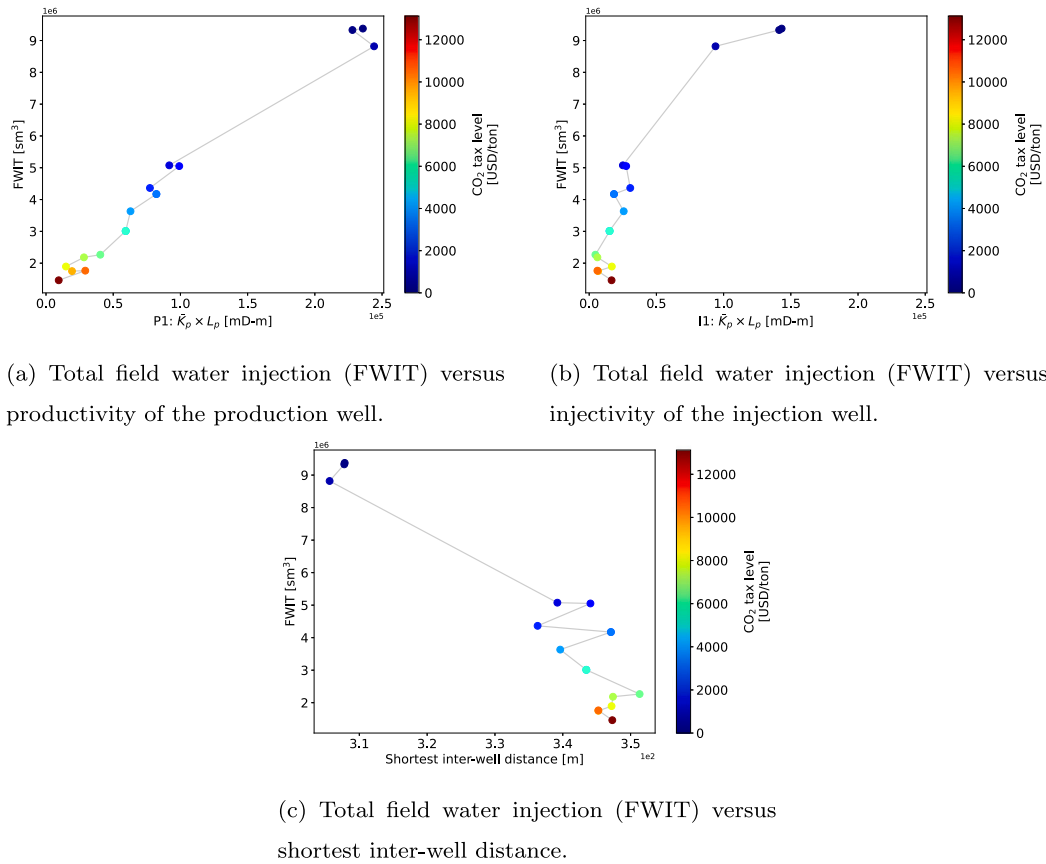


Fig. 8. Relationships between total field water injection and well characteristics obtained from the optimal solutions for our well-placement optimization problems.

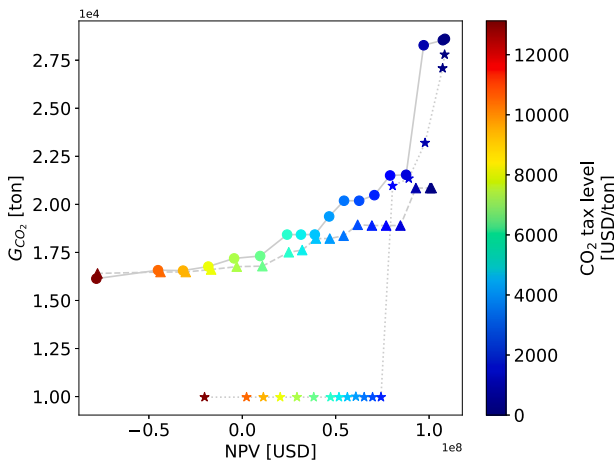


Fig. 9. Relationships between total field CO<sub>2</sub> emissions,  $G_{CO_2}$ , and NPV obtained from three different kinds of optimization problems. The circle markers represent the solutions for the well-placement optimization problems. The triangle markers represent the solutions for the well-placement optimization problems with the reactive well-control measure. The star markers represent the solutions for the joint well-placement-and-control optimization problems. Each marker indicates the CO<sub>2</sub> emissions and NPV that correspond to one optimal solution for one particular CO<sub>2</sub> tax level indicated by the marker color. As in Fig. 7(a), the NPV is calculated using the tax level associated with the solution.

(e.g.,  $r_{CO_2} \geq 2100$  USD/ton), the optimal BHP targets for the production well in year 4–6 are equal to the maximum injection pressure of 420 bar (see the red line in Fig. B.2(a)), causing the field to be shut during that period (see the red line in Fig. 10(a)). This implies that shutting down

the field after some years of production could be more profitable than continuing the field production at high CO<sub>2</sub> taxes. The adjustable well-control enables our joint optimization to stop the field production in an optimal manner. This demonstrates another advantage of incorporating the well-control variables in our joint optimization, i.e., providing extra room for energy efficiency and profitability improvement. The mass rate profile of CO<sub>2</sub> emissions,  $\dot{m}_{CO_2}$ , shown in Fig. 10(b) is similar to the injection rate profile because the injection rate has a larger variation than the injection pressure, thus it dominantly influences the power consumption and the CO<sub>2</sub> emissions.

In the optimal solutions for our joint optimization problems, the relationships between field water injection, oil production, and CO<sub>2</sub> emissions are similar to the one shown in Fig. 5. As a result of shutting down the field in year 4–6 (see the red line in Fig. 10(a)), the optimal drainage strategies for higher CO<sub>2</sub> tax levels manage to reduce the emissions by ~64% with a ~14% drop in oil production. Since the variation of injection pressure is insignificant, the CO<sub>2</sub> emissions remain almost linearly dependent on the water injection volume with an approximate relationship given by:

$$G_{CO_2} = 0.0028 \frac{\text{ton}}{\text{sm}^3} \times \text{FWIT} + 3686 \text{ ton} \quad (3)$$

In addition, if we compare Eq. (3) with Eq. (2), the solutions for our joint optimization often emit less CO<sub>2</sub> than the solutions for the well-placement optimization when injecting the same volume of water, most likely due to the lower injection pressure.

Fig. 11(a) illustrates the variation of injection effectiveness in different optimal solutions. The injection effectiveness of different solutions for our joint optimization problems varies between 0.06 and 0.21, where the solutions for higher CO<sub>2</sub> tax levels tend to have higher effectiveness. In stark contrast to the well-placement optimization, the

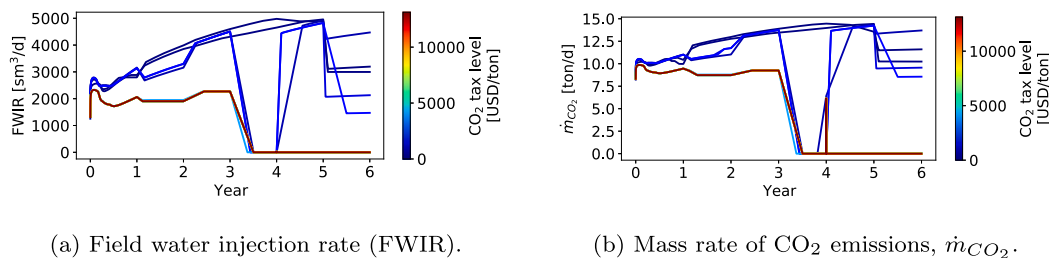


Fig. 10. Profile of field water injection rate and CO<sub>2</sub> emissions throughout the simulated production period with respect to different optimal solutions for our joint optimization problems implementing different CO<sub>2</sub> tax levels.

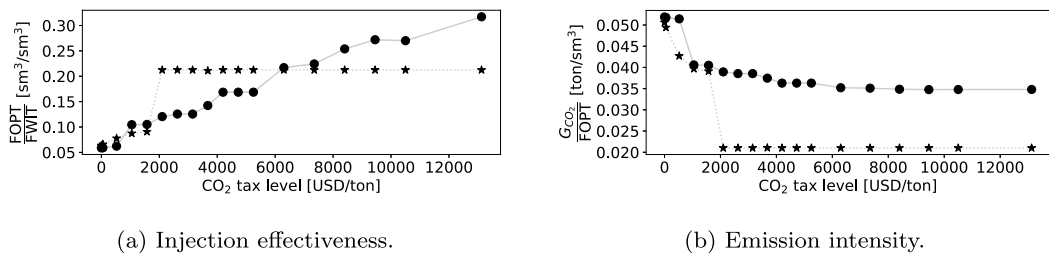


Fig. 11. Injection effectiveness and emission intensity of different optimal solutions for different CO<sub>2</sub> tax levels. The circle markers represent the solutions for the well-placement optimization problems. The star markers represent the solutions for the joint well-placement-and-control optimization problems.

solutions for our joint optimization quickly reach a plateau, where future increases in the CO<sub>2</sub> tax level have no influence on the injection effectiveness. As shown in Fig. 11(b), the solutions for our joint optimization have emission intensity that ranges from 0.021 to 0.051 ton/sm<sup>3</sup>, equivalent to 3.3–8 kg CO<sub>2</sub> per barrel. The use of higher CO<sub>2</sub> tax levels usually results in optimal solutions with lower emission intensity, but there are basically no changes in emission intensity for the CO<sub>2</sub> tax levels above 2100 USD/ton. The CO<sub>2</sub> tax level of 2100 USD/ton is therefore deemed as the critical tax level for our joint optimization study as it results in the lowest emission intensity which cannot be reduced any further. Additionally, for each CO<sub>2</sub> tax level, the solution for our joint optimization has lower emission intensity than that for the well-placement optimization, as expected from the increased degree of freedom in our joint optimization.

In the well-placement optimization, the reductions in water injection and CO<sub>2</sub> emissions are obtained by decreasing the well productivity and injectivity and by increasing the inter-well distance. In the joint optimization, water injection can also be reduced by adjusting the BHP and rate targets for the production and injection wells, respectively. With this additional freedom, it is unnecessary for the joint optimization to lower the well productivity and injectivity in order to reduce the water injection. As shown in Figs. 12(a) and 12(b), the solutions for our joint optimization usually have better well productivity and injectivity than those for the well-placement optimization as shown in Figs. 8(a) and 8(b). The higher well productivity and injectivity could lower the injection pressure. Due to the reduced injection pressure, the solutions for our joint optimization emit less CO<sub>2</sub> than the solutions for the well-placement optimization when injecting the same volume of water. This explains why the solutions for our joint optimization have substantially lower emission intensity despite having similar injection effectiveness as the solutions for the well-placement optimization (see Fig. 11).

Looking at Fig. 12, the optimal solutions for higher CO<sub>2</sub> tax levels entail less water for injection. However, there is no clear trend in injection volume with the variation of well productivity and inter-well distance (see Figs. 12(a) and 12(c)). The change in the inter-well distance is also minor. The reason is that, in the joint optimization, the water injection can also be reduced by adjusting the well-control, thus the injection is no longer solely dependent on the well productivity and the inter-well distance. Referring to Fig. 12(b), the solutions higher CO<sub>2</sub> tax levels tend to have higher well injectivity, contradicting the

trend observed in Fig. 8(b). In the well-placement optimization, the higher well injectivity will increase the injection rate due to the fixed well-control, and thus result in higher emissions. Contrarily in the joint optimization, the higher well injectivity will not necessarily increase the injection rate because the injection rate can be maintained or even reduced by adjusting the well BHP or rate targets. The higher well injectivity indeed implies that we need lower injection pressure for achieving a given rate target, thus resulting in lower emissions. The trend in Fig. 12(b) indicates that the solutions for higher CO<sub>2</sub> tax levels prefer producing oil that is easier to produce, or in other words, that requires lower injection pressure. The trend is the same as the one that appeared in our earlier study (Angga et al., 2022d), i.e., an increase in CO<sub>2</sub> tax level will move the optimal injector placement towards a more permeable area, resulting in lower injection pressure and hence lower CO<sub>2</sub> emissions. Given that the joint optimization solutions are more energy-efficient, the trends in well characteristics concluded from the well-placement solutions (see Fig. 8) could mislead the search for more energy-efficient reservoir drainage as they are considerably different from the trends observed in the joint optimization solutions (see Fig. 12). This indicates the particular importance of our joint optimization study.

We note that the reductions in water injection, oil production, NPV, NPV\*, and CO<sub>2</sub> emissions given in Section 4 are case-dependent, meaning that they might vary on different optimization setups, e.g., on different reservoir models. Despite the magnitude of the reductions being case-dependent, most importantly the trends observed in Section 4 are consistent with the trends observed in our previous studies (Angga et al., 2022b,d,c). One limitation of the present study is related to the optimization runtime, which is quite large even for the relatively small reservoir model employed. Using a single-core standard workstation, the present study entails ~8 and ~31 days for solving the well-placement and joint optimization problems, respectively, on the Egg reservoir model with ~18 000 active cells. To overcome this limitation, industrial applications of the present study (i) could use more computing resources and run all the reservoir simulations involved in each iteration in parallel, (ii) could employ computationally less heavy optimization methods, and (iii) will probably not investigate such a high number of different CO<sub>2</sub> tax levels but restrict themselves to values around the current and probable future tax levels. Another option to deal with the limitation is through the application of proxy models for

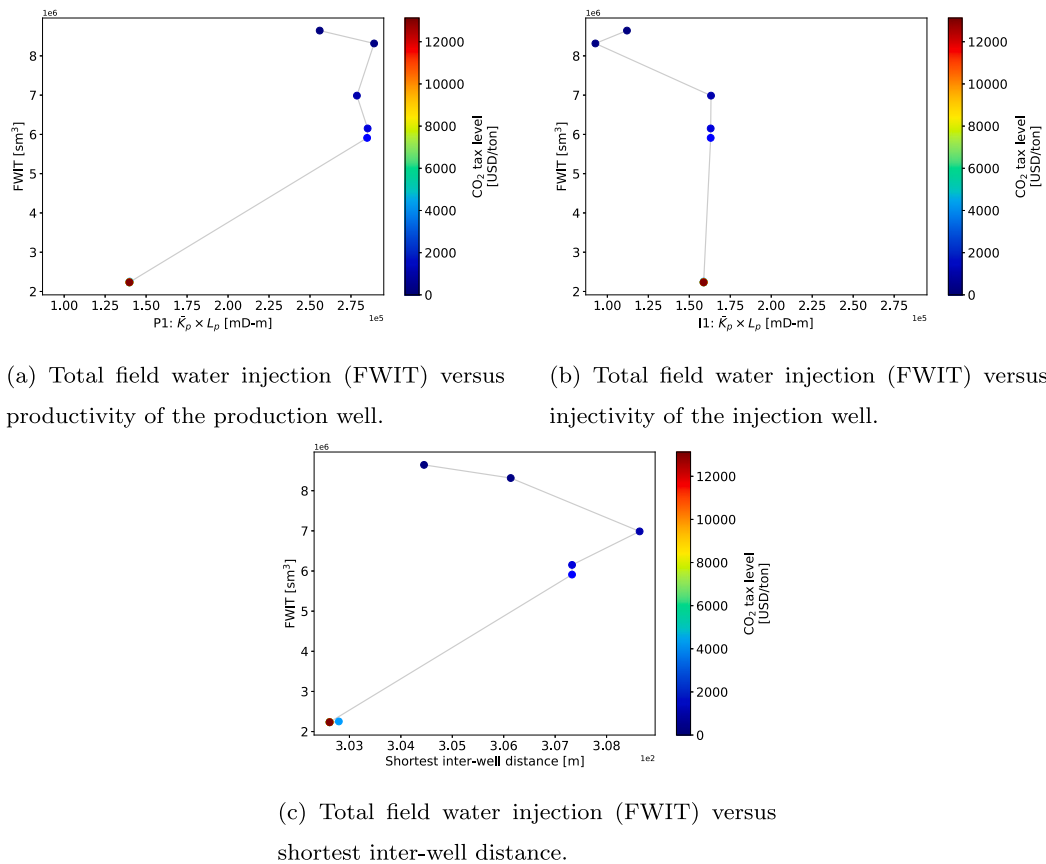


Fig. 12. Relationships between total field water injection and well characteristics obtained from the optimal solutions for our joint optimization problems.

reservoir simulation as demonstrated in Krogstad and Nilsen (2022) and Ng et al. (2021, 2022). These measures could reduce the computational cost drastically and therefore could make the present study robust and feasible for industrial applications. The other limitation is associated with the assumptions made for the CO<sub>2</sub> emission calculator discussed in Angga et al. (2022b).

### 5. Conclusion

This paper presents a study on well-placement and joint well-placement-and-control optimization that is performed on the Egg reservoir model produced with water flooding. The optimization objective takes into account the cost of CO<sub>2</sub> emissions during the water flooding operation. By employing the collaborative algorithm, multiple optimization problems embedding different CO<sub>2</sub> tax levels are solved, aiming to assess the effect of changes in CO<sub>2</sub> tax on the optimal solution. The relationships between water injection, oil production, NPV, and CO<sub>2</sub> emissions are investigated. Well characteristics that contribute to lowering the CO<sub>2</sub> emissions are examined.

The solutions for well-placement and joint optimization share some commonalities as follows: The solutions for higher CO<sub>2</sub> tax levels usually require less water for injection and therefore emit less CO<sub>2</sub>. The emissions and water injection have a linear relationship due to the limited variation in injection pressure. In contrast, the trade-off between emissions and oil production is non-linear where, to a certain extent, we can obtain a solution providing a large emission reduction (e.g., ~29%) with a minimal reduction in oil production (e.g., ~5%). Beyond that, the return on energy efficiency measure diminishes, meaning the same reduction in oil production will give less reduction in emissions due to the reduced opportunities for energy efficiency. The use of higher CO<sub>2</sub> tax levels usually leads to optimal drainage strategies with higher injection effectiveness and lower emission intensity. However, some

increases in CO<sub>2</sub> tax level, particularly above the critical level, have a negligible impact on the optimal solution, hence they will only have a negative effect on the profitability without further reducing the CO<sub>2</sub> emissions or the emission intensity.

Compared to the solutions for our well-placement optimization, the solutions for our joint optimization emit less CO<sub>2</sub> and improve the NPV. The adjustable well-control enables our joint optimization to shut down the field after some years of production which could be more profitable than continuing the field production at high CO<sub>2</sub> taxes. Despite having similar injection effectiveness as the solutions for the well-placement optimization, the solutions for our joint optimization have substantially lower emission intensity due to the lower injection pressure. These three clearly demonstrate the advantages of incorporating the well-control as decision variables, which gives a higher degree of freedom to our joint optimization. In the well-placement optimization with the fixed well-control, the reductions in water injection and CO<sub>2</sub> emissions are only gained by decreasing the well productivity and injectivity and by increasing the inter-well distance. In the joint optimization, the water injection can also be reduced by adjusting the well-control, thus the injection does not solely depend on the well productivity or injectivity and the inter-well distance. This explains why there is no clear trend in well productivity and inter-well distance with the variation of injection volume. Since the well-control is modifiable in the joint optimization, the more energy-efficient solutions conversely tend to have higher well injectivity, aiming to lower the injection pressure and thereby reduce the energy needed for injection. The trends in well characteristics concluded from the well-placement solutions could mislead the search for more energy-efficient drainage as they are considerably different from the trends observed in the joint optimization solutions. This indicates the particular importance of joint optimization in this study.

One limitation of the present study is the lengthy optimization runtime. To reduce the computational cost and make the present study

robust and feasible for industrial applications, one could utilize more computing resources, employ less heavy optimization methods, investigate fewer CO<sub>2</sub> tax levels, and exploit reservoir proxy models.

**Declaration of competing interest**

The authors declare the following financial interests/personal relationships which may be considered as potential competing interests: I Gusti Agung Gede Angga reports financial support was provided by the Research Council of Norway.

**Data availability**

All data used is already open

**Acknowledgment**

The first author, I Gusti Agung Gede Angga, was financially supported by the Research Council of Norway through its Research Centre for Petroleum (PETROSENTER), project number 296207 - LowEmission.

**Appendix A. Optimization parameters**

The coordinates of the eight nodes that define the physical search space in our optimization problems are listed in Table A.1. All parameters for the net present value (NPV) calculation are listed in Table A.2. All parameters for the collaborative genetic algorithm (C-GA) are listed in Table A.3.

**Table A.1**

Coordinates of the eight nodes (in the global Cartesian coordinate system) that define the physical search space in our optimization problems.

Node- <i>i</i>	Global Cartesian coordinate of node- <i>i</i>		
	<i>x<sub>i</sub></i> [m]	<i>y<sub>i</sub></i> [m]	<i>z<sub>i</sub></i> [m]
1	93	54	-4028
2	300	54	-4028
3	300	363	-4028
4	93	363	-4028
5	93	54	-4000
6	300	54	-4000
7	300	363	-4000
8	93	363	-4000

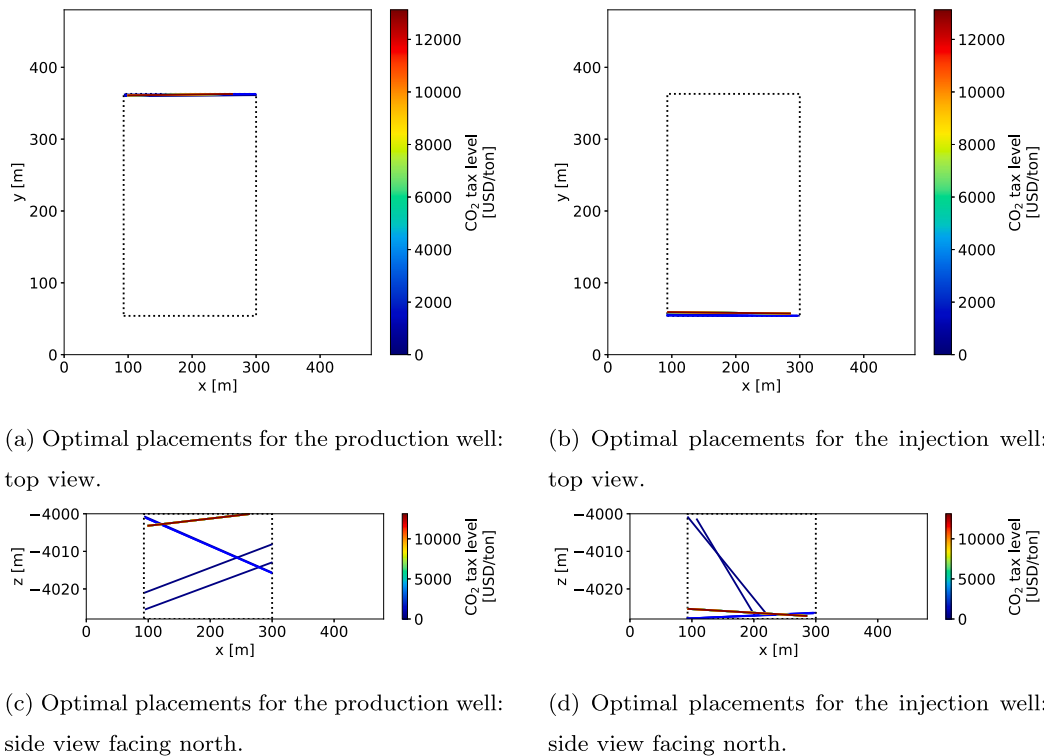


**Fig. B.1.** Optimal placements for the production and injection wells for our joint optimization problems (see Section 3.3). The line color indicates the CO<sub>2</sub> tax level,  $r_{CO_2}$ , that an optimal placement is associated with. The rectangle with dotted outlines denotes the search space in our optimization problems.

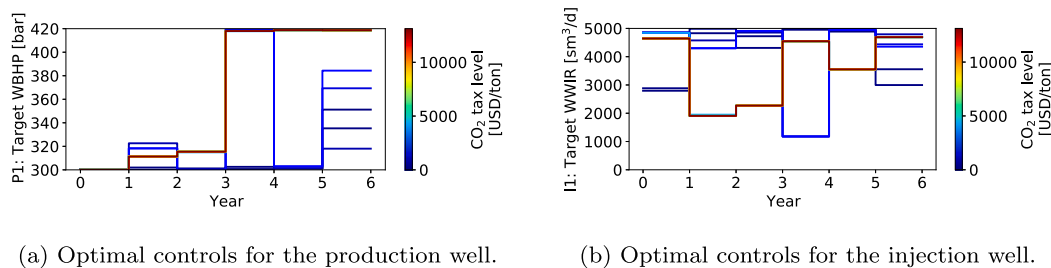


**Fig. B.2.** Optimal controls for the production and injection wells for our joint optimization problems (see Section 3.3).

**Table A.2**  
Parameters for the net present value (NPV) calculation.

Parameter	Value	Description
$C_d$	$5 \times 10^3$ USD/m	The unit cost of drilling.
$P_o$	$3.1445 \times 10^2$ USD/sm <sup>3</sup>	The oil price. It is equivalent to 50 USD/bbl.
$C_w$	$5.0312 \times 10^{-1}$ USD/sm <sup>3</sup>	The unit cost of treating the injected water. It is equivalent to 0.08 USD/bbl.
$C_f$	$1.1613 \times 10^2$ USD/ton	The unit cost of fuel. It is equivalent to the gas price of 2.21 USD/MMBTU given the gas specific energy content of 15.4 MWh/ton (for methane gas).
$r_{CO_2}$	0 – $1.3125 \times 10^4$ USD/ton	The CO <sub>2</sub> tax level. The 18 different CO <sub>2</sub> tax levels involved in this study are 0, $5.25 \times 10^1$ , $5.25 \times 10^2$ , $1.05 \times 10^3$ , $1.575 \times 10^3$ , $2.1 \times 10^3$ , $2.625 \times 10^3$ , $3.15 \times 10^3$ , $3.675 \times 10^3$ , $4.2 \times 10^3$ , $4.725 \times 10^3$ , $5.25 \times 10^3$ , $6.3 \times 10^3$ , $7.35 \times 10^3$ , $8.4 \times 10^3$ , $9.45 \times 10^3$ , $1.05 \times 10^4$ , $1.3125 \times 10^4$ USD/ton.
$d$	8%	The discount rate.
$T$	6 years	The field production period.

**Table A.3**  
Parameters for the collaborative genetic algorithm (C-GA).

Parameter	Value	Description
$N_i$	25 or 50	The number of iterations. It varies depending on the optimization problems. For the well-placement optimization problems described in Section 3.2, $N_i = 25$ . For the joint well-placement-and-control optimization problems described in Section 3.3, $N_i = 50$ .
$N_p$	18	The number of optimization problems to be solved in our MTO. It also indicates the number of populations involved, where one population is devoted to one optimization problem.
$N_m$	$2 \times N_d$	The size of each population. The parameter $N_d$ denotes the number of decision variables that compose the vector $\bar{u}$ .
$p$	$\frac{1}{N_m}$	The proportional parameter needed for the selection operation (see Chuang et al. (2015) for further details).
$\lambda$	0.1	The probability threshold for conducting the crossover operation (see Chuang et al. (2015) for further details).
$\phi_0$	0.25	The bound for random perturbations during the mutation operation (see Chuang et al. (2015) for further details).
$b$	4	The parameter that controls the mutation step size (see Chuang et al. (2015) for further details).
$N_c$	1	The number of promising individuals in other populations to be cloned to a population in each iteration.

## Appendix B. Solutions for the joint optimization

The optimal well-placements and well-controls for our joint optimization problems are illustrated in Figs. B.1 and B.2, respectively.

## References

- Adesina, F.A.S., Churchill, A., Olugbenga, F., 2011. Modeling productivity index for long horizontal well. *J. Energy Resour. Technol.* 133 (3), 033101.
- Al Dossary, M.A., Nasrabadi, H., 2016. Well placement optimization using imperialist competitive algorithm. *J. Pet. Sci. Eng.* 147, 237–248.
- Angga, I.G.A.G., Bellout, M., Bergmo, P.E.S., Slotte, P.A., Berg, C.F., 2022a. Collaborative optimization by shared objective function data. *Array* 16, 100249.
- Angga, I.G.A.G., Bellout, M., Kristoffersen, B.S., Bergmo, P.E.S., Slotte, P.A., Berg, C.F., 2022b. Effect of CO<sub>2</sub> tax on energy use in oil production: waterflooding optimization under different emission costs. *SN Appl. Sci.* 4 (11), 313.
- Angga, I.G.A.G., Bergmo, P.E.S., Berg, C.F., 2022c. Optimization of inflow control valves under different lifting and injection costs. In: *EAGE Conference on Digital Innovation for a Sustainable Future*.
- Angga, I.G.A.G., Sutoyo, H.R.D., Bellout, M., Bergmo, P.E.S., Slotte, P.A., Berg, C.F., 2022d. Effects of well placement on CO<sub>2</sub> emissions from waterflooding operation. In: *SPE Norway Subsurface Conference*.
- Arouri, Y., Lake, L.W., Sayyafzadeh, M., 2022. Bilevel optimization of well placement and control settings assisted by capacitance-resistance models. *SPE J.* 27 (06), 3829–3848.
- Awotunde, A.A., Sibaweih, N., 2014. Consideration of voidage-replacement ratio in well-placement optimization. *SPE Econ. Manag.* 6 (01), 40–54.
- Bathe, K.-J., 1982. *Finite Element Procedures in Engineering Analysis*. Prentice Hall.
- Bellout, M.C., Echeverría Ciaurri, D., Durllofsky, L.J., Foss, B., Kleppe, J., 2012. Joint optimization of oil well placement and controls. *Comput. Geosci.* 16 (4), 1061–1079.
- Chen, H., Feng, Q., Zhang, X., Wang, S., Zhou, W., Geng, Y., 2017. Well placement optimization using an analytical formula-based objective function and cat swarm optimization algorithm. *J. Pet. Sci. Eng.* 157, 1067–1083.
- Chen, H., Feng, Q., Zhang, X., Wang, S., Zhou, W., Liu, C., 2018. Well placement optimization for offshore oilfield based on Theil index and differential evolution algorithm. *J. Pet. Explor. Prod. Technol.* 8 (4), 1225–1233.
- Chen, G., Luo, X., Jiao, J.J., Xue, X., 2022. Data-driven evolutionary algorithm for oil reservoir well-placement and control optimization. *Fuel* 326, 125125.
- Chuang, Y.-C., Chen, C.-T., Hwang, C., 2015. A real-coded genetic algorithm with a direction-based crossover operator. *Inform. Sci.* 305, 320–348.
- Ding, D.Y., 2008. Optimization of well placement using evolutionary algorithms. In: *Europec/EAGE Conference and Exhibition*.
- Farajzadeh, R., Glasbergen, G., Karpan, V., Mjeni, R., Boersma, D.M., Eftekhari, A.A., Casquera Garcia, A., Bruining, J., 2022. Improved oil recovery techniques and their role in energy efficiency and reducing CO<sub>2</sub> footprint of oil production. *J. Clean. Prod.* 369, 133308.
- Farajzadeh, R., Zaal, C., van den Hoek, P., Bruining, J., 2019. Life-cycle assessment of water injection into hydrocarbon reservoirs using exergy concept. *J. Clean. Prod.* 235, 812–821.
- Forouzanfar, F., Poquioma, W.E., Reynolds, A.C., 2016. Simultaneous and sequential estimation of optimal placement and controls of wells with a covariance matrix adaptation algorithm. *SPE J.* 21 (02), 501–521.
- Gupta, A., Ong, Y.-S., Feng, L., 2016. Multifactorial evolution: toward evolutionary multitasking. *IEEE Trans. Evol. Comput.* 20, 343–357.
- Hutahaean, J., Demyanov, V., Arnold, D., Vazquez, O., 2014. Optimization of well placement to minimize the risk of scale deposition in field development. In: *Abu Dhabi International Petroleum Exhibition and Conference*.
- Isebor, O.J., Durllofsky, L.J., Echeverría Ciaurri, D., 2014. A derivative-free methodology with local and global search for the constrained joint optimization of well locations and controls. *Comput. Geosci.* 18 (3), 463–482.
- Islam, J., Vasant, P.M., Negash, B.M., Laruccia, M.B., Myint, M., Watada, J., 2020. A holistic review on artificial intelligence techniques for well placement optimization problem. *Adv. Eng. Softw.* 141, 102767.
- Jansen, J.D., Fonseca, R.M., Kahrobaei, S., Siraj, M.M., Van Essen, G.M., Van den Hof, P.M.J., 2014. The egg model – a geological ensemble for reservoir simulation. *Geosci. Data J.* 1 (2), 192–195.
- Kristoffersen, B.S., Silva, T.L., Bellout, M.C., Berg, C.F., 2022. Efficient well placement optimization under uncertainty using a virtual drilling procedure. *Comput. Geosci.* 26 (4), 739–756.
- Krogstad, S., Nilsen, H.M., 2022. Efficient adjoint-based well-placement optimization using flow diagnostics proxies. *Comput. Geosci.* 26 (4), 883–896.
- Li, L., Jafarpour, B., 2012. A variable-control well placement optimization for improved reservoir development. *Comput. Geosci.* 16 (4), 871–889.

- Li, L., Jafarpour, B., Mohammad-Khaninezhad, M.R., 2013. A simultaneous perturbation stochastic approximation algorithm for coupled well placement and control optimization under geologic uncertainty. *Comput. Geosci.* 17 (1), 167–188.
- Li, M., Wittek, A., Miller, K., 2014. Efficient inverse isoparametric mapping algorithm for whole-body computed tomography registration using deformations predicted by nonlinear finite element modeling. *J. Biomech. Eng.* 136 (8), 0845031–0845036.
- Lu, R., Reynolds, A.C., 2020. Joint optimization of well locations, types, drilling order, and controls given a set of potential drilling paths. *SPE J.* 25 (03), 1285–1306.
- Murti, V., Valliappan, S., 1986. Numerical inverse isoparametric mapping in remeshing and nodal quantity contouring. *Comput. Struct.* 22 (6), 1011–1021.
- Naderi, M., Khamehchi, E., 2017. Application of DOE and metaheuristic bat algorithm for well placement and individual well controls optimization. *J. Nat. Gas Sci. Eng.* 46, 47–58.
- Ng, C.S.W., Jahanbani Ghahfarokhi, A., 2022. Adaptive proxy-based robust production optimization with multilayer perceptron. *Appl. Comput. Geosci.* 16, 100103.
- Ng, C.S.W., Jahanbani Ghahfarokhi, A., Nait Amar, M., 2021. Application of nature-inspired algorithms and artificial neural network in waterflooding well control optimization. *J. Pet. Explor. Prod. Technol.* 11 (7), 3103–3127.
- Ng, C.S.W., Jahanbani Ghahfarokhi, A., Nait Amar, M., 2022. Production optimization under waterflooding with long short-term memory and metaheuristic algorithm. *Petroleum*.
- OG21, 2022. Low-emission technologies. [Online]. Available: [https://www.og21.no/siteassets/dyppykk-2022-lavutslipp/og21\\_report---low-emission-technologies\\_final\\_20221026.pdf](https://www.og21.no/siteassets/dyppykk-2022-lavutslipp/og21_report---low-emission-technologies_final_20221026.pdf).
- Onwunalu, J.E., Durlöfsky, L.J., 2010. Application of a particle swarm optimization algorithm for determining optimum well location and type. *Comput. Geosci.* 14 (1), 183–198.
- OPM, 2022a. Flow. [Online]. Available: [https://opm-project.org/?page\\_id=19](https://opm-project.org/?page_id=19).
- OPM, 2022b. ResInsight. [Online]. Available: [https://opm-project.org/?page\\_id=117](https://opm-project.org/?page_id=117).
- Osaba, E., Del Ser, J., Martinez, A.D., Hussain, A., 2022. Evolutionary multitask optimization: a methodological overview, challenges, and future research directions. *Cogn. Comput.* 14 (3), 927–954.
- Petroleum Cybernetics Group NTNU, 2021. FieldOpt. [Online]. Available: <https://github.com/PetroleumCyberneticsGroup/FieldOpt>.
- Rostamian, A., Jamshidi, S., Zirbes, E., 2019. The development of a novel multi-objective optimization framework for non-vertical well placement based on a modified non-dominated sorting genetic algorithm-II. *Comput. Geosci.* 23 (5), 1065–1085.
- Rystad Energy, 2019. Technologies to improve NCS competitiveness. [Online]. Available: [https://www.og21.no/contentassets/e1765573b1044740ae5425fc27e80dab/technologies-to-improve-ncs-competitiveness\\_rystad-energy\\_final.pdf](https://www.og21.no/contentassets/e1765573b1044740ae5425fc27e80dab/technologies-to-improve-ncs-competitiveness_rystad-energy_final.pdf).
- Sayyafzadeh, M., Alrashdi, Z., 2020. Well controls and placement optimisation using response-fed and judgement-aided parameterisation: Olympus optimisation challenge. *Comput. Geosci.* 24 (6), 2001–2025.
- Semnani, A., Ostadhassan, M., Xu, Y., Sharifi, M., Liu, B., 2021. Joint optimization of constrained well placement and control parameters using teaching-learning based optimization and an inter-distance algorithm. *J. Pet. Sci. Eng.* 203, 108652.
- Siddiqui, M.A., Khan, R.A., Jamal, M.S., 2015. Multi-objective well placement optimization considering energy sustainability along with economical gains. In: *SPE North Africa Technical Conference and Exhibition*.
- Sunday, D., 2021. *Practical Geometry Algorithms: With C++ Code*. Amazon Digital Services LLC.
- Svalheim, S., King, D.C., 2003. Life of field energy performance. In: *SPE Offshore Europe Oil and Gas Exhibition and Conference*.
- Tax Foundation, 2020. Carbon taxes in Europe. [Online]. Available: <https://taxfoundation.org/carbon-taxes-in-europe-2020/>.
- Wang, L., Yao, Y., Zhang, T., Adenutsi, C.D., Zhao, G., Lai, F., 2022. A novel self-adaptive multi-fidelity surrogate-assisted multi-objective evolutionary algorithm for simulation-based production optimization. *J. Pet. Sci. Eng.* 211, 110111.
- Yuan, K.Y., Huang, Y.S., Yang, H.T., Pian, T.H.H., 1994. The inverse mapping and distortion measures for 8-node hexahedral isoparametric elements. *Comput. Mech.* 14 (2), 189–199.
- Yuan, H., Li, W., Yuan, Y., Luo, J., Yan, W., 2021. Productivity evaluation of horizontal well in heterogeneous reservoir with composite water aquifer. *J. Pet. Explor. Prod.* 11 (3), 1363–1373.
- Zhou, P.-L., Cen, S., Huang, J.-B., Li, C.-F., Zhang, Q., 2017. An unsymmetric 8-node hexahedral element with high distortion tolerance. *Internat. J. Numer. Methods Engrg.* 109 (8), 1130–1158.